https://doi.org/10.5194/egusphere-2026-76
Preprint. Discussion started: 16 February 2026

Surface icequakes and basal stick-slip events reveal daily grounding line migration and seawater intrusion at a marine-terminating glacier in East Antarctica

Tifenn Le Bris[1], Guilhem Barruol[1], Florent Gimbert[1], Emmanuel Le Meur[1], Dimitri Zigone[2,3], Maxime Bès de Berc[2], Armelle Bernard[3]

[1] Univ. Grenoble Alpes, CNRS, INRAE, IRD, Grenoble INP, IGE, 38000 Grenoble, France

[2] Université de Strasbourg/CNRS, Institut Terre et Environnement de Strasbourg, UMR7063, 67084 Strasbourg Cedex, France

[3] Université de Strasbourg/CNRS, Ecole et Observatoire des Sciences de la Terre, UAR830, 67084 Strasbourg Cedex, France

Correspondence to: Tifenn Le Bris (tifenn.le-bris@univ-grenoble-alpes.fr)

Abstract. As they reach the ocean, Antarctic outlet glaciers transition from grounded to floating at their so-called grounding lines (GL). This transition is known to be mechanically controlled by tides, which induce ice flexure visible at the surface from satellite and ground geodesy and often used as a proxy for grounding line position. Here, we use a dense seismic node array to study the spatial and temporal dynamics of surface, crevasse-induced icequake activity and basal, sliding-induced seismicity at the grounding zone of the Astrolabe Glacier, a fast-moving outlet glacier in East Antarctica. We observe that surface icequakes mimic the expected, tide-induced, ice flexure pattern, as they delineate the grounding line position inferred from previous geodetic studies, and migrate landward as tides rise. We show, however, that the mechanical grounded to floating transition is better evidenced by the spatial distribution of basal sliding-induced stick-slip events, occurring on a limited number of clusters and which depict a grounding line position that is offset inland compared to that identified from the surface. These basal events undergo tidally-driven cycles of activation and de-activation, consistent with sea water intrusion inland over at least 3 kilometers at high tides. Following these results, we propose that the monitoring of stick-slip events could be used as the most accurate means of tracking grounding line retreat over long timescales.

https://doi.org/10.5194/egusphere-2026-76
Preprint. Discussion started: 16 February 2026

1 Introduction

The Antarctic ice sheet naturally flows towards the ocean through outlet glaciers that meet the ocean at their grounding lines (GL), which represent the boundary between grounded ice sheet and floating ice shelves. Foundational studies have shown that variations in grounding line position strongly influence ice mass loss (Rignot et al., 2011; Schoof, 2007; Vaughan, 1994). As the grounding line retreats toward the continent, for instance by the effect of basal melting and ice thinning, the reduction in buttressing effect allows faster ice flow, increasing ice mass loss and ultimately contributing to sea level rise. Improving projections of future sea-level rise therefore requires a more detailed understanding of the processes and boundary conditions that govern grounding lines positions and dynamics.

While we tend to focus on the long-term changes for sea-level projections, a major control on grounding line dynamics may occur at a short time scale under the response of the glacier to the daily and sub-daily tidal forcing. Tide-induced variations in sea level height cause indeed a vertical up-and-down displacement of the floating ice and therefore a horizontal back-and-forth migration of the grounding line, forming a dynamic area at the ice-bedrock interface called grounding zone (GZ) (Freer et al., 2023; Rignot et al., 2024). This daily migration changes the coupling state at the ice-bedrock interface, modulating the glacier basal sliding behavior (Christmann et al., 2021; Yan et al., 2024). Rising water pressure during high tides is expected to lubricate the bed and to enhance sliding (Gagliardini et al., 2007; Lliboutry, 1968; Schoof, 2005), while falling tides increase basal friction at the ice-bedrock interface (Robel et al., 2017). This tidal "breathing" is also expected to generate strong subglacial ocean water advection that may enhance ocean-ice interaction and basal melt processes.

A range of observational techniques, including satellite altimetry, radar interferometry (InSAR), optical imagery, airborne and terrestrial radar systems, have expanded our capabilities to track grounding line positions, down to meter-scale spatial resolution (e.g., Bindschadler et al., 2011). However, their uneven and sparse temporal data coverages limit the high temporal resolution analysis needed for studying daily GL migration and associated changes in basal conditions (Mohajerani et al., 2021). Altimetry data from ICESat observations revealed tide-induced flexure of the southern Ronne Ice Shelf and, by combining multiple tracks spread over several years, enabled regional-scale estimates of tidally driven GL migration at different tide heights (Freer et al., 2023). Similarly, daily DInSAR observations from the ICEYE constellation captured short-term GL migration at the main trunk of Thwaites Glacier (Rignot et al., 2024). Yet, neither approaches provide continuous grounding line position time series or constraints on basal friction states. Both are however essential to fully capture GL behavior over tidal cycles (Friedl et al., 2020; Rignot et al., 2011a) and to provide constraints on the tidal pumping effect that could enhance ice-ocean thermal exchanges and basal melting at GL (Begeman et al., 2020; Gadi et al., 2023; Walker et al., 2013).

By its ability to detect and locate events generated by ice friction and brittle deformation, cryoseismology is a good candidate for such continuous and high resolution monitoring of grounding line dynamics. Among cryoseismic signals recorded at outlet glaciers, tide-modulated icequakes occurring close to the surface have been linked to temporal and spatial variations in stress from the glacier cyclic bending in response to tidal forcing on sea-level height (e.g. Barruol et al., 2013; Cooley et al., 2019; Fromm et al., 2023; Hulbe et al., 2016;

https://doi.org/10.5194/egusphere-2026-76
Preprint. Discussion started: 16 February 2026

Le Bris et al., 2025; Lombardi et al., 2016). When recorded by a dense seismic array, icequakes also demonstrated their ability to provide a means of delineating the grounding line (Le Bris et al., 2025).

Seismic events at the ice-bed interface reveal the complementary mechanisms of glaciers sliding over the bedrock. The so-called stick-slip events have been observed across a variety of glacial environments, including Antarctic ice streams (Anandakrishnan & Alley, 1997; Barcheck et al., 2018; Danesi et al., 2007; Hudson et al., 2023; Kufner et al., 2021; Winberry et al., 2013; Zoet et al., 2012), Greenland Ice Sheet (McBrearty et al., 2020; Roeoesli et al., 2016) and Alpine glaciers (Gräff et al., 2021; Helmstetter et al., 2015; Hudson et al., 2020). In some cases of coastal ice streams and outlet glaciers, tidal cycles have been demonstrated to modulate basal seismicity, with periodic basal stress changes triggering stick-slip behavior (Pratt et al., 2014; Walter et al., 2015; Winberry et al., 2009; Zoet et al., 2012). However, no direct means of monitoring grounding line migration from these events has yet been established.

Through the combined analysis of surface icequakes and basal stick-slip seismicity, this study aims at providing direct insights into the grounding line position and migration at daily timescales. By using a dense array of seismic nodes deployed over the grounding zone of an outlet glacier from East Antarctica, we detect and determine the temporal and spatial distribution of both types of events recorded during consecutive daily tidal cycles and investigate how tide-induced surface brittle deformation and changes in frictional conditions at the ice-bedrock interface are connected to the grounding line dynamics.

2 Data

2.1 Study site

The Astrolabe Glacier (Terre Adélie, East Antarctica) is an outlet glacier located next to the Dumont d'Urville (DDU) research station. It has been the site of several studies including GNSS, radar and seismology surveys, all focused on constraining the glacier dynamics (Barruol et al., 2025, submitted, Le Bris et al., 2025; Le Meur et al., 2014; Provost et al., 2024). Figure 1 presents the site location. The floating part of the Astrolabe Glacier is laterally constrained within a fjord with valley walls estimated to be at least 500 to 600 m deep, covered by grounded stable ice. In some areas of the GZ, the thickness of the floating tongue has been estimated at approximately 700 m, gradually thinning to around 300 m at its terminus (Le Meur et al., 2014). With only limited direct observations, these values likely vary along the glacier. In front of the terminus, sparse bathymetric surveys offshore (Beaman et al., 2011) show that the fjord bathymetry extends deeper than 1,000 m, suggesting a large subglacial cavity beneath the floating ice tongue, prone to ocean intrusion and ice basal melting. The current grounding line position (Fig. 1a) has been determined by integrating ice thickness data defining the line of buoyant flotation with kinematic GPS measurements of vertical motion due to tidal flexure (Le Meur et al., 2014).

https://doi.org/10.5194/egusphere-2026-76
Preprint. Discussion started: 16 February 2026

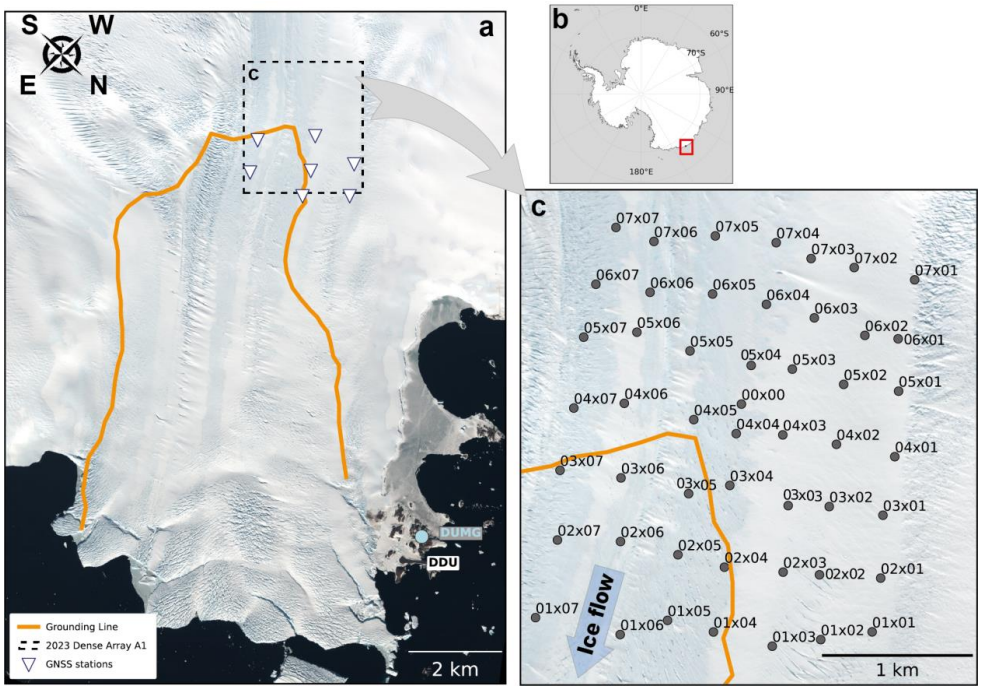

Figure 1: 2023 seismic deployment on the Astrolabe Glacier, East Antarctica. (a) Map of the Astrolabe Glacier region, near the French base station Dumont d'Urville (DDU). The background image is a Pleiades satellite acquisition from January 10, 2025. The dotted black rectangle indicates the locations of the 2023 dense seismic array and includes the GNSS permanent stations (white triangles) and the DUMG reference station. The orange line represents the "geodetic" grounding line as estimated by Le Meur et al. (2014). (b) Location of the study area along the East Antarctica coast. (c) Close-up view of the 2023 deployment: 50 seismic nodes (black dots) installed across the grounding zone.

2.2 Observations: dense array of seismic nodes, GNSS and tide data

During the Austral summer 2023, a dense seismic node array was deployed on the Astrolabe Glacier using SmartSolo IGU-16HR 3C instruments (Barruol et al., 2025, submitted). The deployment consisted of 50 three-component stations installed across the grounding zone (Fig. 1c). The array operated continuously from 10th Jan. 2023 to 02nd Feb. 2023, with a sampling rate of 500 Hz. The inter-station spacing averages 400 m, covering an area of approximately 7 km². This configuration was designed to resolve fine-scale seismic sources along the transition from grounded to floating ice. Seismic nodes were inserted into drilled snow pits approximately 50 cm deep and covered with compacted snow to favor re-freezing around them. We observed an expected horizontal station displacement up to ~ 20 m, over the deployment period.

We collected ground-based GNSS measurements at 7 sites on the glacier, using multifrequency Trimble NetR9 receivers and Trimble Zephyr Geodetic antennas (Fig. 1a). We processed GNSS phase observables, sampled at 30 s intervals, in kinematic mode using the TRACK software (Chen, 1999; Herring et al., 2018) and using

https://doi.org/10.5194/egusphere-2026-76
Preprint. Discussion started: 16 February 2026

multiple GNSS constellations (GPS, GLONASS, and Galileo). The position of the survey sites on the glacier was determined with respect to the reference station DUMG installed at the close-by Dumont d'Urville site (Fig. 1a).

Sea level height is obtained using the PM36S MarArgos automatic tide gauge DUMON, installed at the DDU base (NIVMER/ROSAME project, Calzas et al., 1992). The sampling interval is 2 minutes. The daily tidal pattern alternates between diurnal cycles (one high tide per 24 hours) and mixed diurnal cycles. In mixed diurnal cycles, the dominant high tide reaches 1.5-2 m amplitude, while the secondary high tide amplitude is much smaller, on the order of only a few tens of centimeters.

3 Methods

3.1 Icequakes detection, occurrence and location

Icequakes are impulsive seismic events broadly accepted to be generated by brittle fracturing within the ice (Lewandowska and Teisseyre, 1964; Neave and Savage, 1970; Osten-Woldenburg, 1990; Röthlisberg, 1955; Röthlisberger, 1972). These events generally dominate the seismic records by their amplitudes. Their waveforms are characterized by a lack of clear P- or S-wave onsets or distinguishable seismic phases. They often exhibit a dominant frequency content between 5 and 40 Hz. Here, we apply the same method as Le Bris et al. (2025) to detect icequakes in the continuous time series using a standard Short-Term Average over Long-Term Average (STA/LTA) algorithm (Allen, 1978; Lesage, 2009). We perform the detection on the vertical component of the seismic signal band-pass filtered between 5 Hz and 40 Hz with the following detection parameters: STA = 0.5 seconds; LTA = 5 seconds; trigger-on and off thresholds set to 5 and 2, respectively.

We detect thousands of low-magnitude icequakes across the dense array area. To assess the spatial variations of the icequake activity, we adopt a statistical approach. This is particularly relevant here, as we overcome the challenge of locating icequakes using standard methods which fail to accurately pick phases, likely due to surface crevassing affecting the waveforms (Le Bris et al., 2025). For each station, we compute the icequake occurrence rates, defined as the number of events detected in a two-hour window. Occurrence rates observed at each node are then spatially interpolated over the array surface using a kriging method (Cressie, 1993; Kitanidis, 1997) (Text S1, Suppl. Inf.). Here, we compute occurrence rates over seven consecutive 24-hour tidal cycles, from January 17 to 24, 2023 and then average and interpolate the occurrence rates to build a time series extending over a single representative 24-hour tidal cycle.

3.2 Stick-slip events detection and location

Stick-slip events are pervasively present in the seismic data but have amplitudes overall three times smaller than the icequakes. They are characterized by their short duration (typically <1 second), high frequency content (25–100 Hz), and highly repetitive waveforms with distinct P- and S-wave arrivals (Fig. 2a) suggesting an extremely constant source and focal mechanism. In the raw waveform data, they appear as bursts of repeating signals occurring at very constant time intervals and clustered over several hours (Fig. 2b).

https://doi.org/10.5194/egusphere-2026-76
Preprint. Discussion started: 16 February 2026

Our stick-slip detection methodology operates in three main steps. First, through visual inspection of the continuous seismic data, we select a template characterized by clear P- and S-phases (Gräff et al., 2021; Helmstetter et al., 2015; Hudson et al., 2023; Roeoesli et al., 2016). The window is typically 0.5 s long. Second, using a Template Matching Detection approach, we look for events matching the selected template over the full time series of one station showing the best signal quality. We consider a detection as a potential stick-slip event if the correlation is above 0.65. This threshold is chosen based on the correlation coefficient gaussian distribution of manually checked events, which decays exponentially below 0.65. Finally, we limit false positive detections by performing visual comparison of all events detected, with the mean waveform computed from averaging events with highest correlation coefficient (usually above 0.95 to ensure very little variations in waveform amplitude between events) (Fig. 2a). If some of the false positives have similar characteristics to the template but show different waveforms, they are classified as new clusters, and are then used as templates to detect associated events. Similar methods have frequently been used to detect basal events, with correlation coefficient thresholds depending on whether a more cautious (higher threshold) or more exhaustive (lower threshold) approach is chosen (Allstadt and Malone, 2014; Carmichael et al., 2012; Helmstetter et al., 2015; Mikesell et al., 2012; Thelen et al., 2013).

We then locate clusters of stick-slips using the Python package QuakeMigrate (Hudson et al., 2020, Winder et al., 2020). Due to the wide spacing between seismic stations (~400 m), S-wave arrivals are often difficult to observe (Fig. 2c), such that we only rely on P-wave arrivals for initial location. As a consequence, the initial depth estimates carry high uncertainty (Fig. 2d). To refine it, we perform a grid search around the initial QuakeMigrate location on stacked waveforms which better resolve S-wave arrivals (Fig. 2e). We test different source positions to minimize the misfit between observed and predicted source-receiver distances. To evaluate the misfit, we compute the Root Mean Square Error (RMSE) using the following equation:

$$RMSE = \sqrt{\frac{\sum_{i=1}^{M} (\Delta d_{pred_i} - \Delta d_{obs_i})^2}{M}}, \quad (1)$$

where M is the number of stations used to constrain the RMSE and Δd_{pred} and Δd_{obs} are respectively the predicted and observed source-station distance with

$$\Delta d_{obs_i} = (T_S - T_P)_i \times \frac{(V_P \times V_S)}{(V_S - V_P)}, \quad (2)$$

where T_P and T_S are the P-wave and S-wave arrival times, and V_P and V_S the P-wave and S-wave velocities. We manually pick P- and S- wave arrival times from stacked waveforms, where the S-wave is made more visible (as shown in Fig. 2e).

We perform the grid search in the 6 dimensions X, Y, Z, V_P, V_S and $(T_S - T_P)$, where (X, Y, Z) vary within a 2 km x 2 km x 1 km cube around the initial source location, V_P in the range 3,800 - 4,000 m/s and V_S in the range 1,700 –1,900 m/s (Llorens et al., 2020; Wittlinger and Farra, 2012). This refinement reduces the uncertainty for the depth estimate, giving a more confident location (Fig. 2f). We account for picking error by performing the grid search with $(T_S - T_P)$ varying within an uncertainty of ± 8 ms. For clusters where S-wave arrivals are too difficult to pick precisely, even after stacking, no depth is assigned (around 24% of the clusters).

https://doi.org/10.5194/egusphere-2026-76
Preprint. Discussion started: 16 February 2026

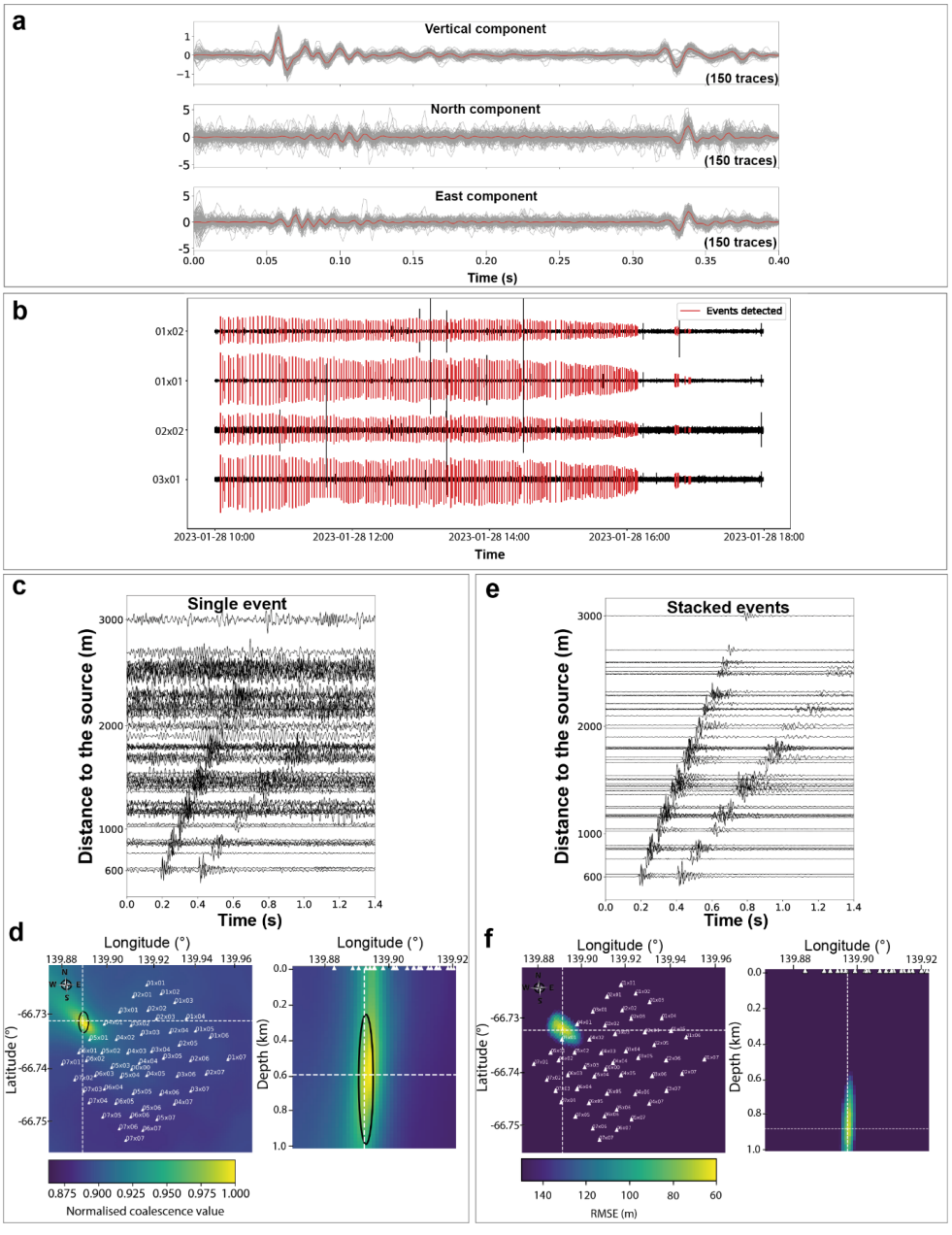

Figure 2: Stick-slip detection and location procedure. (a) Stacked waveform (red) from a cluster of stick- slip events (cluster 15), as observed at station 03x01 on the three components. Individual normalized waveforms from the cluster (150 traces) are shown in grey, highlighting the high waveform similarity within the cluster. (b) Eight-hour window of
195 **continuous seismic data on Jan. 28, 2023 from four stations (03x01, 02x02, 01x01, and 01x02), on the vertical component, during a period of activity for cluster 15. Red segments indicate individual detections identified via template matching with the selected cluster template. Amplitudes are independently normalized for each station. (c)**

https://doi.org/10.5194/egusphere-2026-76
Preprint. Discussion started: 16 February 2026

Waveforms of a single event from cluster 15 (vertical component) recorded at the 50 stations plotted as a function of epicentral distance from the cluster source location. Seismograms are filtered between 25 and 100Hz. (d) Location of cluster 15 based on QuakeMigrate (Winder et al., 2020). Normalised coalescence value represents how well seismic arrivals from all stations "stack" coherently at a given point in the 3D grid. (e) Stacked waveforms of 767 events from cluster 15 (vertical component) at the 50 stations plotted as a function of epicentral distance from the cluster source location. Seismograms are filtered between 25 and 100Hz. (f) Refined location of cluster 15 from grid search. RMSE value is based on the difference between observed and modeled time arrival of P and S waves from manual picking.

4 Results

4.1 Migration of the grounding zone over tidal cycle: surface icequakes signature

Figure 3 presents a series of maps showing the interpolated icequake activity across the dense array during the different stages of a tidal cycle. The grounding line as identified geodetically by Le Meur et al. (2014) separates the grounded ice (top section and right corner of the array) and the floating ice (lower left corner of the array). At low tide (Fig. 3a), icequake activity is weak and concentrated on the east side of the array, showing no apparent link with the position of the grounding line. At mid-rising tide (Fig. 3b), the icequake activity migrates within the floating ice area, consistent with the grounding line position. At high tide (Fig. 3c), icequake activity intensifies over the floating area but also migrates upstream, in the opposite direction to the ice flow, well beyond the grounding line position. At falling tide (Fig. 3d and e), the icequake activity is still high but no longer matches the grounding line position, instead diffusing over the dense array without a clear pattern. At the end of the cycle (10h after the high tides) the icequake levels decrease and go back to the initial levels (Fig. 3a). Vertical displacement from GNSS stations (colored triangles in Fig. 3) confirm the uplift movement during rising to high tide and downlift movement during falling to low tide, coherent with tidal flexuring. Vertical displacement across GNSS stations shows higher displacement magnitude for northeastmost stations located on the floating tongue of the glacier (i.e. GPS08, GPS03 and GPS02). Figure 3f focuses on a single day, the 18th of January 2023, when icequake activity is highest, likely due to high tide (spring tides) and to low noise level that day. We draw the contour of the average icequake activity rate for each hour from mid-rising (-6h) to high tide (0h). During this small time window, this map reveals an extremely dynamic migration of the icequake activity from approximately the “geodetic” grounding line position extending landward to both the northwest (with a lateral migration of less than 1km) and southwest directions (with an upstream, along-flow migration of more than 2 km).

https://doi.org/10.5194/egusphere-2026-76
Preprint. Discussion started: 16 February 2026

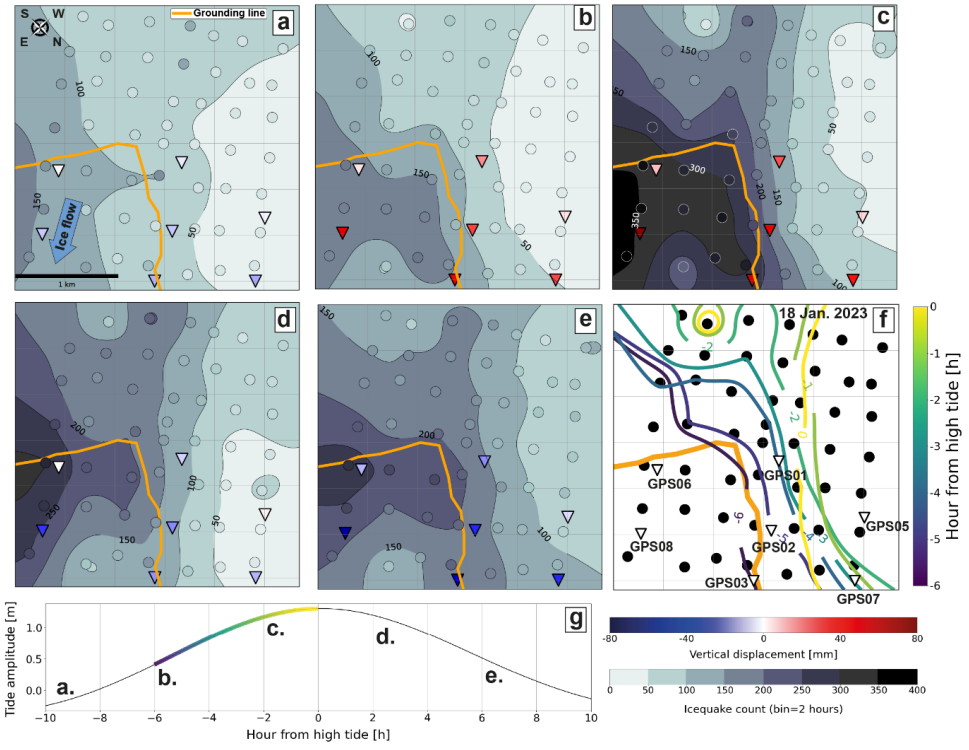

Figure 3: (a) to (e): Spatial distribution of icequake activity across the dense seismic array during a tidal cycle. The maps are derived from kriging-based interpolation of icequake occurrence rates, averaged over seven consecutive tidal cycles from January 17 to 24, 2023. Icequake occurrence rates are expressed as the average number of events per 2-hour interval. Darker shades correspond to higher icequake occurrence rates. Each panel represents a 2-hour interval within the 12-hour window leading up to and following high tide. The corresponding time slot is reported on the tidal amplitude graph, reconstructed from the seven consecutive tidal cycles. For each window, the GNSS stations are colored according to the measured vertical displacement. (f) Contour of the average icequake activity for each hour from mid-rising to high tide observed on 18th Jan. 2023. (g) Tidal amplitude on 18 January 2023 over a 20-hour window centered on high tide. The positions of panels (a–e) are shown according to their respective tidal stage. The colors used in panel (f) are referenced on the tidal curve to indicate each hourly interval from mid-rising tide to high tide.

4.2 Stick-slip dynamics at the grounding zone during tidal cycles

Stick-slip locations

The number of events detected for each stick-slip cluster and the source coordinates are summarized Table S1 (Suppl. Inf.). Clusters have a wide range of activity, from 40 to more than 4000 individual events detected in a week, with a total of more than 24,000 individual stick-slip events. We present in Figure 4a the map with the location of the 29 stick-slip clusters detected within the deployment duration, along with their estimated depths for 22 of them. The striking feature is that all the detected clusters are located at the periphery or outside of the network with no event detected beneath it. This suggests the absence of seismically active gliding at the ice-

https://doi.org/10.5194/egusphere-2026-76
Preprint. Discussion started: 16 February 2026

bedrock interface in this area, consistent with a floating ice shelf. Several clusters located at the periphery of the network outline the east and west lateral shear margins of the glacier. Along the west lateral shear margin, depths vary from 225 m to 915 m. Beneath the east lateral shear margin, clusters with reliable depth estimates are generally deeper, ranging from 800 m to 1,300 m. Additionally, we locate clusters upstream of the dense array. Some of these clusters are aligned along the glacier flow and associated with depths greater than 1,300m. The other clusters are shallower, at maximum 660 m depth, and aligned perpendicular to the flow. The estimated source depths are generally consistent with the broad bedrock topographic trends outlined in previous radar surveys conducted in the area (Le Meur et al., 2014), but tend to be larger by a few hundred meters. Despite reliable identification of both P- and S-wave arrivals, the absolute depth remains uncertain due to poor constraints on seismic velocities and the fact that most event clusters are located outside the array aperture. We explore the trade-off between the depth estimate and the seismic velocities, which shows that the depth can vary several hundred meters depending on the (Vp, Vs) couple chosen (see Fig. S1, Suppl. Inf). We further show that the overestimation can be mitigated by inferring seismic velocities that fall outside the typical range reported for glacier ice, and particularly by using slower shear velocities (e.g., 1400m/s) than investigated in the present study. It emphasizes the need for independent measurements of seismic velocities to better constrain the stick-slips and therefore the bedrock depth estimates but has no impact on the following of the discussion.

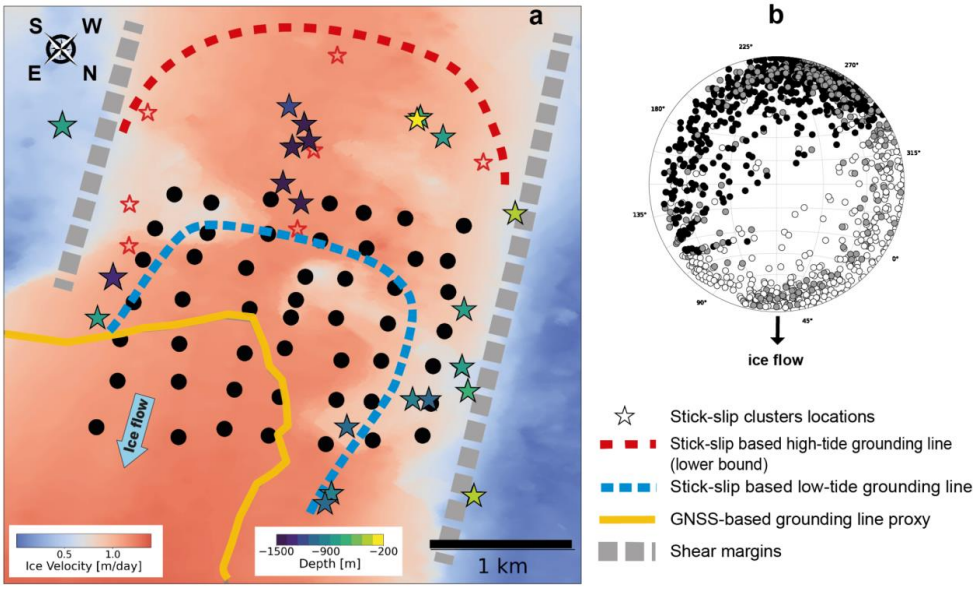

Figure 4: Stick-slip clusters location. (a) Map showing the locations of 29 detected stick-slip clusters (stars), overlaid on the ice surface horizontal velocity map from Provost et al. (2024). Clusters are color-coded by their depths. Red stars indicate clusters with poorly resolved depths. The continuous orange line represents the "geodetic" grounding line from Le Meur et al. (2014). The detected stick-slip clusters allow to define a grounding zone bounded by a low and a high tide grounding line, indicated by the blue and red dotted lines, respectively. (b) Lower hemisphere

https://doi.org/10.5194/egusphere-2026-76
Preprint. Discussion started: 16 February 2026

stereonet representing the upward (black circles) and downward (white circles) first P-wave motion over the whole network. Grey circles indicate unsure polarisation.

Stick-slip occurrence

To investigate the dynamics of stick-slip events over tidal cycles and identify patterns in their activation, we first analyse the number of clusters active at the same time during the deployment period (Fig. 5a) and then quantify four key parameters variation along a virtual single tide cycle: number of active clusters (Fig. 5b), event counts (Fig. 5c), inter-event time (Fig. 5d), and event amplitude (Fig. 5e). In each case, we focus on the period from 17 to 24 January 2023, and values are averaged over 30-minute bins, and presented over a single 24-hours tidal cycle.

We observe that the activation of the clusters is clearly modulated by the tides (Fig. 5a). Over the whole week of the time series, we observe the number of simultaneously active clusters increasing from low to rising tides (around 5 to 7), then rapidly decreasing from high to falling tides (below 2). When averaged over the 8 days (Fig. 5b) the number of simultaneous active clusters peaks at more than 4 at rising tides and decreases to 1 at falling tides. The associated total number of individual stick-slip events per 30 min (Fig. 5c) shows a rather similar trend, which culminates at 600 events during rising tides, decreases at high tide, and is the lowest during falling tide (at about 100 events). 80% of the clusters exhibit a clear tidal pattern while the remaining, mostly located on the east shear margin, show relatively constant event counts across the tidal cycle. The icequake activity presented as the red curve on the same diagram displays a clearly different pattern with a bimodal distribution, with a first peak at rising tide and a second at falling tide, as already shown in more details on Fig. 8b from Le Bris et al. (2025). The average inter-event time (IET) between stick-slip events typically ranges between 4 and 8 minutes (Fig. 5d), with a slight decrease during the falling-to-low tide phase, reaching values below 4 minutes. This trend suggests a rather stable activity with a slight acceleration of stick-slip occurrence as the tide recedes. It is consistent with the surface GNSS measurements that show an horizontal acceleration of the glacier during falling tide (Fig. 11 from Le Bris et al., 2025). No systematic correlation is found between inter-event times and spatial location. We quantify the mean event amplitude over 30-minutes bins, by extracting the maximum of the envelope of the signals within the stick-slip events time window and across all stations. We then calculate the average amplitude to represent the event as viewed by the full network. To decouple amplitude variation from events occurrence, we normalize the amplitudes by the total number of events in the 30-minutes bin. Figure 5e clearly shows that stick-slip amplitudes vary with tides: they increase during rising tide, peak at high tide, and decrease during falling tide. This observation is consistent across all clusters. The rather stable inter-event times and the larger number of events at rising tide suggest that more energy is released per event at high tide to accommodate the ice flow.

https://doi.org/10.5194/egusphere-2026-76
Preprint. Discussion started: 16 February 2026

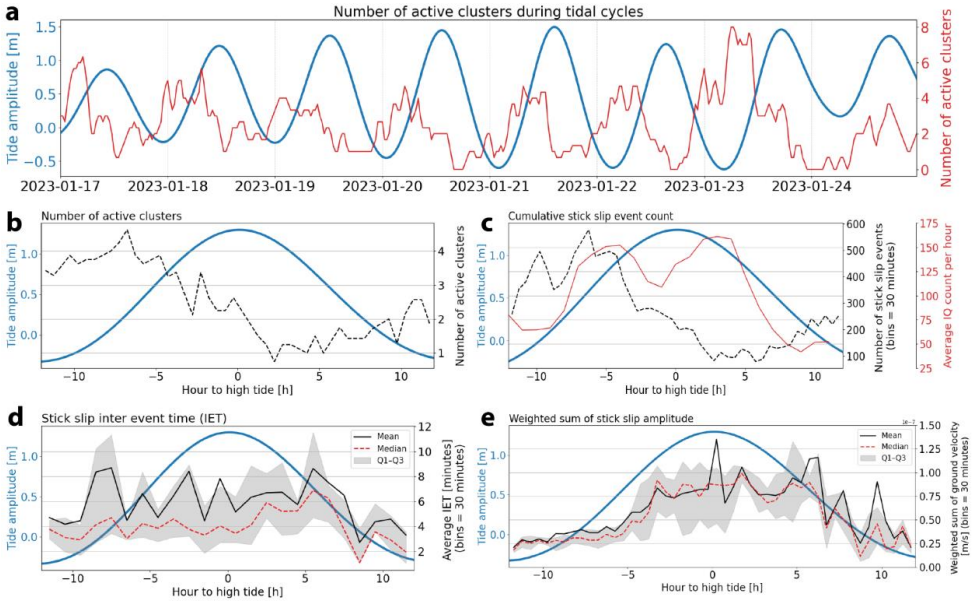

Figure 5: Stick-slip activity relative to tide. (a) Time series of the number of active stick-slip clusters (red curve) over the period 17–24 January 2023, together with the tide amplitude (blue curve). (b) number of active clusters (black curve) folded over a representative 24-hour tidal cycle, divided into 30-minute bins. The x-axis represents time relative to high tide, from –12 to +12 hours and tidal amplitude is plotted as a blue curve. Values from all clusters are concatenated. (c) Total number of stick-slip events from all clusters along with the average icequake activity rate (in count per hour, red curve). (d) stick-slip inter-event time (IET). (e) event amplitudes (ground velocity, in m/s). For IET and event amplitudes, the mean (black curve), median (red dotted curve), and interquartile range (25th–75th percentiles displayed in grey shading) are shown.

Stick slip focal mechanism

We analyse the focal mechanism of each cluster by locating compressional (up) or dilatational (down) motions across the seismic network, which in turn allows identification of the nodal planes and fault geometry (vertical strike-slip, normal, reverse, or oblique). To do so, we stacked the waveforms of all events within each cluster across all seismic nodes of the dense array, in order to make the P-wave first motions more visible. Three analysts independently identified the first motions, classified as “up,” “down,” or “uncertain”. For each cluster, the identifications were then combined with unanimity in the agreement on the “up” or “down” motion provided by the 3 analysts. When analyzing P-wave first motions for fault mechanism determination, the ideal scenario is a full azimuthal and incidence angle coverage around the seismic source. Here, we are unfortunately limited by partial azimuthal and inclination coverage of the seismic sources relative to the stations, since most of them occur at the periphery of the network, thus impeding to cover the whole azimuth/inclination hemisphere and hence resolving the full focal mechanisms. To overcome this limitation, we make the hypothesis that all clusters have similar focal mechanisms and merge all the compressional and dilatational wave motions into a single virtual source displayed in the stereonet Fig. 4b. We obtain a clear two-quadrant mechanism, with

https://doi.org/10.5194/egusphere-2026-76
Preprint. Discussion started: 16 February 2026

compressional upward first motions southward and dilatational downward first motions northward in the lower hemisphere. This coherent pattern confirms our initial hypothesis that all stick-slip clusters share a similar focal mechanism (for individual stereonets, see Fig. S2, Suppl. Inf.). At first approximation, such quadrant configuration is compatible with a horizontal strike-slip faulting and an along-flow displacement. We observe a slight obliquity between the azimuth of the vertical focal plane and the flow direction that could likely reflect departure from a flat and horizontal bedrock hypothesis, such as dipping and laterally-varying structures.

5 Discussion

Surface icequakes as a proxy for grounding line migration

During rising tide, we observe that the zone of intense surface icequake activity migrates landward, opposite to the direction of ice flow (Fig. 3). These icequakes being the brittle response to the tide-induced flexure of the glacier at its GZ (Le Bris et al., 2025), this suggests that the flexure moves upstream during rising tides. We quantify that the upstream migration of icequake activity at the glacier surface occurs at an apparent velocity ranging from 0.1 to 0.3 m/s. This velocity is controlled by the amplitude of the tidal flexure of the glacier but also by the bedrock slope, which is poorly constrained in our region. The same order of magnitude has been observed by Rignot et al. (2024) at the Thwaites Glacier with grounding line migration velocity of 0.5 m/s. Assuming that such flexure is closely related to the seawater intrusion at its base (Gadi et al., 2023; Rack et al., 2017; Robel et al., 2017; Walker et al., 2013), one can deduce that the minimum horizontal distance of seawater intrusion observed beneath the Astrolabe Glacier GZ is 3 km, the approximate length of the array. We could expect seawater to travel greater distance landward, depending on the topography of the bed, which is unknown. Such value is compatible with other studies revealing either tidal flexuring observations several kilometers beyond the grounding line (uplift visible up to a cm-scale) (Drews et al., 2021) or grounding line migration at a kilometer-scale over tidal cycles (Chen et al., 2023; Ciracì et al., 2023; Millan et al., 2020). Our ability to constrain the intrusion distance from tidal flexure observation is however limited not only by the spatial extent of the seismic network, but more critically by the fact that the surface flexure is a proxy that may sign with some offset with the processes occurring directly at the glacier base.

A new delineation of the grounding zone based on stick-slip clusters

Using stick-slip clusters of events at the base of the glacier, we show that we can constrain the true mechanical grounding line position and its temporal migration. It is broadly accepted that stick-slip events originate from basal friction and accommodate sliding at the ice-bedrock interface or on bedrock asperities, either at the glacier base or along the lateral shear margins where differential motion occurs. In principle, stick-slip sources are expected to occur upstream of the grounding line where the glacier is expected to be at least partially grounded, the glacier being fully floating downstream of the GL. However, in our observations, such events are absent directly beneath the dense array (supposedly at least partially grounded) and instead appear significantly upstream of it (Fig. 4). Consequently, this suggests that the grounding line may lie farther inland from the "geodetic", flexure-induced, grounding line proposed by Le Meur et al. (2014). The activation pattern of stick-slip clusters (Fig. 5a) further supports this interpretation: maximum cluster activities are observed at rising tides, when enough stress has been accumulated. Then, clusters deactivate at high tide, consistent with ice surrection

https://doi.org/10.5194/egusphere-2026-76
Preprint. Discussion started: 16 February 2026

and seawater intrusion reducing bed-ice contact. Stick-slip clusters reactivate during low tides, when renewed contact reestablishes basal friction and will allow the glacier flow to start a new cycle of shear stress concentration at some pinning points of the ice-bedrock interface. Based on these observations, we delineate a new grounding zone using stick-slip activity (Fig. 4a), bounded by a lower (downstream) limit (blue dashed line Fig. 4a) at low tide (when clusters are active) and an upper (upstream) limit (red dashed line Fig. 4a) at high tide (when they are absent). This upper limit is conservative since it could extend further inland but is limited by our ability to detect stick-slip activity at larger distances from the node array. This stick-slip derived grounding zone shows a clear offset relative to both the previously proposed "geodetic" grounding line and the position inferred from tidal-induced icequake activity. Importantly, stick-slip analysis maps the mechanical grounding line, defined by direct ice-bedrock contact, rather than the flexural grounding line seen from the surface of the glacier or from space. While the flexural grounding line is a good proxy that reflects the surface bending, it is inherently offset from the true basal mechanical boundary.

Constraining grounding zone dynamics

In accordance with observations from surface icequakes and stick-slip events, we propose, in Figure 6a, a conceptual model illustrating the grounding zone dynamics at a daily tidal cycle scale: as the tide begins to rise, it lifts up the floating part of the glacier inducing seawater to infiltrate the subglacial cavity. This transitional phase may destabilize the ice-bedrock interface by changing its state of effective pressure and thus triggering stick-slip sources by releasing the accumulated stress at the bedrock on sub-horizontal fault planes. At the same time, the tide-induced bending of the glacier generates an extensional state of stress and numerous icequakes at the surface, migrating landward together with the flexure migration. At high tide, seawater intrusion has reduced friction and deactivated most of the stick-slip sources by lubricating or opening the ice-bedrock interface. The stick-slip activity becomes concentrated in only a few locations, still seismically accommodating the glacier horizontal flow, with less frequent but more energetic events. During falling tide, stick-slip activity is minimal. This suggests that the interface is still lubricated from the preceding high tide and/or that the accumulated stress is not yet high enough to generate seismic events. It allows for smoother, aseismic basal and lateral sliding with reduced resistance from bedrock asperities. As the system reaches low tide, seawater has drained toward the cavity, leading to a reduction in lubrication of the interface and starting a new cycle of increased basal contacts resulting in a new cycle of stress accumulation and in a higher rate of small stick-slip events.

https://doi.org/10.5194/egusphere-2026-76
Preprint. Discussion started: 16 February 2026

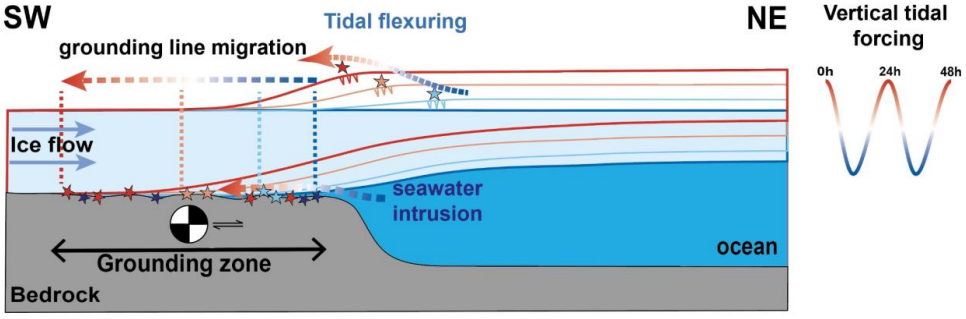

Figure 6: Cartoon of the seismic observations and interpretation of grounding zone dynamics during a tidal cycle. It includes the surface icequakes generated by the tidal flexure, the grounding line migration and seawater intrusion seen by the basal stick-slip events. Note that the vertical movement is not to scale.

Tracking grounding line retreat using seismology

Overall, both surface icequakes and stick-slip clusters provide constraints on grounding zone dynamics. Surface icequakes, driven by tidal flexure, migrate landward in response to grounding line motion. It can help mapping grounding line position from surface activity although with a systematic offset relative to its actual location at the ice base. At the ice-bedrock interface, daily tidal cycles modulate grounding line migration through seawater intrusion, which governs the activation, deactivation, and magnitude of stick-slip events. Following such observations, we propose that the monitoring of stick-slip clusters could offer a direct means of tracking grounding line retreat over long timescales. This is of particular importance considering the first-order control of the basal friction and of pinning points on the coastal glacier stability (e.g., (Pirli et al., 2018)). Unlike geodetic methods, which are limited to surface observations, recording of seismicity captures processes over the whole ice column down to the glacier base, at high spatial and temporal resolution. Once clusters are identified and located, a monitoring strategy may focus on a single or a little number of active clusters using a reduced but efficient seismic setup: a little number of surface stations may be indeed enough to monitor a cluster activity over long time periods. The eventual disappearance of stick-slip clusters could sign a grounding line retreat and/or a basal melting and ice thinning. This makes the approach a low-cost, low-maintenance, yet powerful tool for multi-annual monitoring of grounding line retreat.

6 Conclusion

We describe the dynamic of the coastal Astrolabe Glacier at its GZ in response to consecutive tidal cycles, capturing fine-scale spatial and temporal variability of cryo-seismic events occurring both at the surface and at the ice-bedrock interface. Our observations show that surface brittle deformation migrates landward during rising tide, suggesting that tidal flexuring propagates inland in direct correlation with grounding line migration and associated seawater intrusion. These icequakes may thus serve as a strong proxy for monitoring grounding line migration on daily timescales. In addition, we also detect and locate stick-slip clusters at the ice-bedrock interface, activated and modulated by the tidal cycle: numerous clusters of low-energy events occur during low tides, while fewer but higher-energy events are concentrated at high tides. This pattern aligns with seawater

https://doi.org/10.5194/egusphere-2026-76
Preprint. Discussion started: 16 February 2026

intrusion during rising tides, reducing basal friction and/or removing the direct contact between ice and bedrock, and increased basal friction rates at receding tides when seawater is retreating. Together, these results provide new insights into the high temporal and spatial resolution of grounding line migration driven by tidal, flexure-induced glacier deformation. This deformation is detected by surface icequakes and basal stick-slips, the latter of which show a clear upstream offset and underlie the actual mechanical grounding line. Such observations are valuable for constraining future models of glacier and grounding line dynamics under tidal forcing. They will also become crucial for monitoring Antarctic ice sheet vulnerability to warm water intrusion at grounding zones of outlet glaciers, and particularly for constraining the tidal pumping effect which may enhance ocean-ice interaction and the subsequent basal melting.

Data availability

The SEIS-ADELICE seismic data are available at the EPOS-France data center under the FDSN network code ZR (Barruol et al. 2023). Raw and processed GNSS data acquired on the Astrolabe Glacier GZ are available under a Creative Commons Attribution 4.0 International license in Togaibekov et al. (2024). Tide gauge data, managed by the NIVMER/ ROSAME project (Calzas et al., 1992), are available at https://doi.org/10.17183/REFMAR#108. Seismic data were processed using ObsPy version 1.4.0 (Beyreuther et al., 2010; The ObsPy Development Team, 2022), available under the ObsPy license at https://docs.obspy.org/. Figures were made with Matplotlib version 3.5.3 (Caswell et al., 2020; Hunter, 2007), available under the Matplotlib license at https://matplotlib.org/. All data and scripts used to generate the figures and results in this study are openly available under a Creative Commons Attribution 4.0 International license. The full dataset, including icequakes detection, stick-slip clusters detection and location, metadata, and scripts, is archived in Le Bris (2025).

Author contributions

TLB, GB, and FG conceptualized the study. AB and MBdB curated the data. TLB conducted the investigation and performed the formal analysis, visualization, and original draft writing. All authors (TLB, GB, FG, ELM, DZ, AB, and MBdB) contributed to review and editing of the manuscript. DZ and ELM provided resources. GB and FG supervised the research. GB secured funding and administered the project.

Competing interests

The authors declare that they have no conflict of interest.

Acknowledgements

The SEIS-ADELICE project benefited from the support of the French Polar Institute Paul-Émile Victor (IPEV) for the program #1214, from the French CNRS-INSU SYSTER and LEFE-IMAGO programs, from the Grenoble University UGA-IRGA funding, for the project NODES-ADELICE supported by the French National Research Agency (ANR) in the framework of the "Investissements d'avenir" program (ANR-15-IDEX-02), from the LabEx OSUG@2020 (Investissements d'avenir – ANR10 LABX56) for the project DAS-ADELICE,

https://doi.org/10.5194/egusphere-2026-76
Preprint. Discussion started: 16 February 2026

and from IGE Grenoble. We are grateful to EPOS-France (European Plate Observing System https://www.epos-france.fr/) for the data management. Seismic nodes used in this study have been provided by the "Plateforme instrumentale sismologique" of EOST and complemented by nodes from IPGP (Institut de Physique du Globe de Paris). Thanks to Louis Grauwin, Enzo Tahon, Léonard Barthélémy, Arnaud Reboud, Tom Dumouch for their efficient help in the field work. Thanks to Pierre Rizzardo from ENSA Chamonix for his help and for securing the January 2023 field work on the Astrolabe Glacier. Thanks to P. Techine, M. Calzas and L. Testut for providing access to the tide gauge data managed by the NIVMER/ ROSAME project.

References

Allen, R. V.: Automatic earthquake recognition and timing from single traces, Bull. Seismol. Soc. Am., 68, 1521–1532, https://doi.org/10.1785/BSSA0680051521, 1978.

Allstadt, K. and Malone, S. D.: Swarms of repeating stick-slip icequakes triggered by snow loading at Mount Rainier volcano, J. Geophys. Res. Earth Surf., 119, 1180–1203, https://doi.org/10.1002/2014JF003086, 2014.

Anandakrishnan, S. and Alley, R. B.: Tidal forcing of basal seismicity of ice stream C, West Antarctica, observed far inland, J. Geophys. Res. Solid Earth, 102, 15183–15196, https://doi.org/10.1029/97JB01073, 1997.

Barcheck, C. G., Tulaczyk, S., Schwartz, S. Y., Walter, J. I., and Winberry, J. P.: Implications of basal micro-earthquakes and tremor for ice stream mechanics: Stick-slip basal sliding and till erosion, Earth Planet. Sci. Lett., 486, 54–60, https://doi.org/10.1016/j.epsl.2017.12.046, 2018.

Barruol, G., Cordier, E., Bascou, J., Fontaine, F. R., Legrésy, B., and Lescarmontier, L.: Tide-induced microseismicity in the Mertz glacier grounding area, East Antarctica, Geophys. Res. Lett., 40, 5412–5416, https://doi.org/10.1002/2013GL057814, 2013.

Barruol, G., & Zigone, D., & RESIF: SEIS-ADELICE temporary experiment measuring the cryoseismicity of the Astrolabe glacier in Terre Adelie, Antarctica (RESIF-SISMOB), RESIF - Réseau Sismologique et géodésique Français [Data set], https://doi.org/10.15778/RESIF.ZR2020, 2023

Beaman, R. J., O'Brien, P. E., Post, A. L., and Santis, L. D.: A new high-resolution bathymetry model for the Terre Adélie and George V continental margin, East Antarctica, Antarct. Sci., 23, 95–103, https://doi.org/10.1017/S095410201000074X, 2011.

Begeman, C. B., Tulaczyk, S., Padman, L., King, M., Siegfried, M. R., Hodson, T. O., and Fricker, H. A.: Tidal Pressurization of the Ocean Cavity Near an Antarctic Ice Shelf Grounding Line, J. Geophys. Res. Oceans, 125, e2019JC015562, https://doi.org/10.1029/2019JC015562, 2020.

Bindschadler, R., Choi, H., Wichlacz, A., Bingham, R., Bohlander, J., Brunt, K., Corr, H., Drews, R., Fricker, H., Hall, M., Hindmarsh, R., Kohler, J., Padman, L., Rack, W., Rotschky, G., Urbini, S., Vornberger, P., and Young, N.: Getting around Antarctica: new high-resolution mappings of the grounded and freely-floating boundaries of the Antarctic ice sheet created for the International Polar Year, The Cryosphere, 5, 569–588,

https://doi.org/10.5194/egusphere-2026-76
Preprint. Discussion started: 16 February 2026

https://doi.org/10.5194/tc-5-569-2011, 2011.

Calzas, M., Techine, P., & Testut, L. : Nivmer, https://doi.org/10.18142/135, 1992

Carmichael, J. D., Pettit, E. C., Hoffman, M., Fountain, A., and Hallet, B.: Seismic multiplet response triggered by melt at Blood Falls, Taylor Glacier, Antarctica, J. Geophys. Res. Earth Surf., 117, https://doi.org/10.1029/2011JF002221, 2012.

Caswell, T., Lee, A., Droettboom, M., Sales de Andrade, E., Hoffmann, T., Klymak, J., et al.: Matplotlib V3.5.3, Zenodo [Software], https://doi.org/10.5281/zenodo.6982547

Chen, G.: GPS kinematic positioning for the airborne laser altimetry at Long Valley, California, Thesis, Massachusetts Institute of Technology, 1999.

Chen, H., Rignot, E., Scheuchl, B., and Ehrenfeucht, S.: Grounding Zone of Amery Ice Shelf, Antarctica, From Differential Synthetic-Aperture Radar Interferometry, Geophys. Res. Lett., 50, e2022GL102430, https://doi.org/10.1029/2022GL102430, 2023.

Christmann, J., Helm, V., Khan, S. A., Kleiner, T., Müller, R., Morlighem, M., Neckel, N., Rückamp, M., Steinhage, D., Zeising, O., and Humbert, A.: Elastic deformation plays a non-negligible role in Greenland's outlet glacier flow, Commun. Earth Environ., 2, 232, https://doi.org/10.1038/s43247-021-00296-3, 2021.

Ciracì, E., Rignot, E., Scheuchl, B., Tolpekin, V., Wollersheim, M., An, L., Milillo, P., Bueso-Bello, J.-L., Rizzoli, P., and Dini, L.: Melt rates in the kilometer-size grounding zone of Petermann Glacier, Greenland, before and during a retreat, Proc. Natl. Acad. Sci., 120, e2220924120, https://doi.org/10.1073/pnas.2220924120, 2023.

Cooley, J., Winberry, P., Koutnik, M., and Conway, H.: Tidal and spatial variability of flow speed and seismicity near the grounding zone of Beardmore Glacier, Antarctica, Ann. Glaciol., 60, 37–44, https://doi.org/10.1017/aog.2019.14, 2019.

Cressie, N.: Statistics for spatial data, (Vol. Wiley Series in Probability and Statistics), 137 pp., 1993.

Danesi, S., Bannister, S., and Morelli, A.: Repeating earthquakes from rupture of an asperity under an Antarctic outlet glacier, Earth Planet. Sci. Lett., 253, 151–158, https://doi.org/10.1016/j.epsl.2006.10.023, 2007.

Drews, R., Wild, C. T., Marsh, O. J., Rack, W., Ehlers, T. A., Neckel, N., and Helm, V.: Grounding-Zone Flow Variability of Priestley Glacier, Antarctica, in a Diurnal Tidal Regime, Geophys. Res. Lett., 48, e2021GL093853, https://doi.org/10.1029/2021GL093853, 2021.

Freer, B. I. D., Marsh, O. J., Hogg, A. E., Fricker, H. A., and Padman, L.: Modes of Antarctic tidal grounding line migration revealed by Ice, Cloud, and land Elevation Satellite-2 (ICESat-2) laser altimetry, The Cryosphere, 17, 4079–4101, https://doi.org/10.5194/tc-17-4079-2023, 2023.

https://doi.org/10.5194/egusphere-2026-76
Preprint. Discussion started: 16 February 2026

Friedl, P., Weiser, F., Fluhrer, A., and Braun, M. H.: Remote sensing of glacier and ice sheet grounding lines: A review, Earth-Sci. Rev., 201, 102948, https://doi.org/10.1016/j.earscirev.2019.102948, 2020.

Fromm, T., Schlindwein, V., Helm, V., and Fofonova, V.: Observing tidal effects on the dynamics of the Ekström Ice Shelf with focus on quarterdiurnal and terdiurnal periods, J. Glaciol., 1–11, https://doi.org/10.1017/jog.2023.4, 2023.

Gadi, R., Rignot, E., and Menemenlis, D.: Modeling Ice Melt Rates From Seawater Intrusions in the Grounding Zone of Petermann Gletscher, Greenland, Geophys. Res. Lett., 50, e2023GL105869, https://doi.org/10.1029/2023GL105869, 2023.

Gagliardini, O., Cohen, D., Råback, P., and Zwinger, T.: Finite-element modeling of subglacial cavities and related friction law, J. Geophys. Res. Earth Surf., 112, https://doi.org/10.1029/2006JF000576, 2007.

Gräff, D., Köpfli, M., Lipovsky, B. P., Selvadurai, P. A., Farinotti, D., and Walter, F.: Fine Structure of Microseismic Glacial Stick-Slip, Geophys. Res. Lett., 48, e2021GL096043, https://doi.org/10.1029/2021GL096043, 2021.

Helmstetter, A., Nicolas, B., Comon, P., and Gay, M.: Basal icequakes recorded beneath an Alpine glacier (Glacier d'Argentière, Mont Blanc, France): Evidence for stick-slip motion?, J. Geophys. Res. Earth Surf., 120, 379–401, https://doi.org/10.1002/2014JF003288, 2015.

Herring, T. A., King, R. W., Floyd, M. A., and McClusky, S. C.: Introduction to GAMIT/GLOBK, Massachusetts Institute of Technology, 2018.

Hudson, T. S., Brisbourne, A. M., Walter, F., Gräff, D., White, R. S., and Smith, A. M.: Icequake Source Mechanisms for Studying Glacial Sliding, J. Geophys. Res. Earth Surf., 125, e2020JF005627, https://doi.org/10.1029/2020JF005627, 2020.

Hudson, T. S., Brisbourne, A. M., Kufner, S.-K., Kendall, J.-M., and Smith, A. M.: Array processing in cryoseismology, Ice sheets/Instrumentation, https://doi.org/10.5194/egusphere-2023-657, 2023a.

Hudson, T. S., Kufner, S. K., Brisbourne, A. M., Kendall, J. M., Smith, A. M., Alley, R. B., Arthern, R. J., and Murray, T.: Highly variable friction and slip observed at Antarctic ice stream bed, Nat. Geosci., 1–7, https://doi.org/10.1038/s41561-023-01204-4, 2023b.

Hulbe, C. L., Klinger, M., Masterson, M., Catania, G., Cruikshank, K., and Bugni, A.: Tidal bending and strand cracks at the Kamb Ice Stream grounding line, West Antarctica, J. Glaciol., 62, 816–824, https://doi.org/10.1017/jog.2016.74, 2016.

Kitanidis, P. K.: Introduction to Geostatistics: Applications in Hydrogeology, Cambridge University Press, 276 pp., 1997.

Kufner, S.-K., Brisbourne, A. M., Smith, A. M., Hudson, T. S., Murray, T., Schlegel, R., Kendall, J. M.,

https://doi.org/10.5194/egusphere-2026-76
Preprint. Discussion started: 16 February 2026

Anandakrishnan, S., and Lee, I.: Not all Icequakes are Created Equal: Basal Icequakes Suggest Diverse Bed Deformation Mechanisms at Rutford Ice Stream, West Antarctica, J. Geophys. Res. Earth Surf., 126, e2020JF006001, https://doi.org/10.1029/2020JF006001, 2021.

Le Bris, T., Barruol, G., Gimbert, F., Le Meur, E., Zigone, D., Togaibekov, A., Lombardi, D., Bès de Berc, M., and Bernard, A.: Spatial and Temporal Variability in Tide-Induced Icequake Activity at the Astrolabe Coastal Glacier, East Antarctica, J. Geophys. Res. Earth Surf., 130, e2024JF008054, https://doi.org/10.1029/2024JF008054, 2025.

Le Bris, T.: DATA of ' Surface Icequakes and Basal Stick-Slip Events Reveal Daily Grounding Line Migration and Seawater Intrusion at a Marine-Terminating Glacier in East Antarctica', Zenodo [Data set], https://doi.org/10.5281/zenodo.17977426, 2025

Le Meur, E., Sacchettini, M., Garambois, S., Berthier, E., Drouet, A. S., Durand, G., Young, D., Greenbaum, J. S., Holt, J. W., Blankenship, D. D., Rignot, E., Mouginot, J., Gim, Y., Kirchner, D., de Fleurian, B., Gagliardini, O., and Gillet-Chaulet, F.: Two independent methods for mapping the grounding line of an outlet glacier – an example from the Astrolabe Glacier, Terre Adélie, Antarctica, The Cryosphere, 8, 1331–1346, https://doi.org/10.5194/tc-8-1331-2014, 2014.

Lesage, P.: Interactive Matlab software for the analysis of seismic volcanic signals, Comput. Geosci., 35, 2137–2144, https://doi.org/10.1016/j.cageo.2009.01.010, 2009.

Lewandowska and Teisseyre: Investigations of the ice microtremors on Spitsbergen in 1962, Biul Inf Kom. Wypraw Geof PAN 37 1-5, 1964.

Lliboutry, L.: General Theory of Subglacial Cavitation and Sliding of Temperate Glaciers, J. Glaciol., 7, 21–58, https://doi.org/10.3189/S0022143000020396, 1968.

Llorens, M.-G., Griera, A., Bons, P. D., Gomez-Rivas, E., Weikusat, I., Prior, D. J., Kerch, J., and Lebensohn, R. A.: Seismic Anisotropy of Temperate Ice in Polar Ice Sheets, J. Geophys. Res. Earth Surf., 125, e2020JF005714, https://doi.org/10.1029/2020JF005714, 2020.

Lombardi, D., Benoit, L., Camelbeeck, T., Martin, O., Meynard, C., and Thom, C.: Bimodal pattern of seismicity detected at the ocean margin of an Antarctic ice shelf, Geophys. J. Int., 206, 1375–1381, https://doi.org/10.1093/gji/ggw214, 2016.

McBrearty, I. W., Zoet, L. K., and Anandakrishnan, S.: Basal seismicity of the Northeast Greenland Ice Stream, J. Glaciol., 66, 430–446, https://doi.org/10.1017/jog.2020.17, 2020.

Mikesell, T. D., van Wijk, K., Haney, M. M., Bradford, J. H., Marshall, H. P., and Harper, J. T.: Monitoring glacier surface seismicity in time and space using Rayleigh waves, J. Geophys. Res. Earth Surf., 117, https://doi.org/10.1029/2011JF002259, 2012.

Millan, R., St-Laurent, P., Rignot, E., Morlighem, M., Mouginot, J., and Scheuchl, B.: Constraining an Ocean

https://doi.org/10.5194/egusphere-2026-76
Preprint. Discussion started: 16 February 2026

Model Under Getz Ice Shelf, Antarctica, Using A Gravity-Derived Bathymetry, Geophys. Res. Lett., 47, e2019GL086522, https://doi.org/10.1029/2019GL086522, 2020.

Mohajerani, Y., Jeong, S., Scheuchl, B., Velicogna, I., Rignot, E., and Milillo, P.: Automatic delineation of glacier grounding lines in differential interferometric synthetic-aperture radar data using deep learning, Sci. Rep., 11, 4992, https://doi.org/10.1038/s41598-021-84309-3, 2021.

Murphy, B., Yurchak, R., and Müller, S.: GeoStat-Framework/PyKrige: v1.7.2, , https://doi.org/10.5281/zenodo.11360184, 2024.

Neave, K. G. and Savage, J. C.: Icequakes on the Athabasca Glacier, J. Geophys. Res. 1896-1977, 75, 1351–1362, https://doi.org/10.1029/JB075i008p01351, 1970.

Osten-Woldenburg, H. V. D.: Icequakes On Ekström Ice Shelf Near Atka Bay, Antarctica, J. Glaciol., 36, 31–36, https://doi.org/10.3189/S0022143000005517, 1990.

Pirli, M., Hainzl, S., Schweitzer, J., Köhler, A., and Dahm, T.: Localised thickening and grounding of an Antarctic ice shelf from tidal triggering and sizing of cryoseismicity, Earth Planet. Sci. Lett., 503, 78–87, https://doi.org/10.1016/j.epsl.2018.09.024, 2018.

Pratt, M. J., Winberry, J. P., Wiens, D. A., Anandakrishnan, S., and Alley, R. B.: Seismic and geodetic evidence for grounding-line control of Whillans Ice Stream stick-slip events, J. Geophys. Res. Earth Surf., 119, 333–348, https://doi.org/10.1002/2013JF002842, 2014.

Provost, F., Zigone, D., Le Meur, E., Malet, J.-P., and Hibert, C.: Surface dynamics and history of the calving cycle of Astrolabe Glacier (Adélie Coast, Antarctica) derived from satellite imagery, The Cryosphere, 18, 3067–3079, https://doi.org/10.5194/tc-18-3067-2024, 2024.

Rack, W., King, M. A., Marsh, O. J., Wild, C. T., and Floricioiu, D.: Analysis of ice shelf flexure and its InSAR representation in the grounding zone of the southern McMurdo Ice Shelf, The Cryosphere, 11, 2481–2490, https://doi.org/10.5194/tc-11-2481-2017, 2017.

Rignot, E., Mouginot, J., and Scheuchl, B.: Antarctic Grounding Line Mapping from Differential Satellite Radar Interferometry, Geophys Res Lett, 38, https://doi.org/10.1029/2011GL047109, 2011a.

Rignot, E., Mouginot, J., and Scheuchl, B.: Ice Flow of the Antarctic Ice Sheet, Science, 333, 1427–1430, https://doi.org/10.1126/science.1208336, 2011b.

Rignot, E., Ciracì, E., Scheuchl, B., Tolpekin, V., Wollersheim, M., and Dow, C.: Widespread seawater intrusions beneath the grounded ice of Thwaites Glacier, West Antarctica, Proc. Natl. Acad. Sci., 121, e2404766121, https://doi.org/10.1073/pnas.2404766121, 2024.

Robel, A. A., Tsai, V. C., Minchew, B., and Simons, M.: Tidal modulation of ice shelf buttressing stresses, Ann. Glaciol., 58, 12–20, https://doi.org/10.1017/aog.2017.22, 2017.

https://doi.org/10.5194/egusphere-2026-76
Preprint. Discussion started: 16 February 2026

Roeoesli, C., Helmstetter, A., Walter, F., and Kissling, E.: Meltwater influences on deep stick-slip icequakes near the base of the Greenland Ice Sheet: DEEP STICK-SLIP ICEQUAKES OF THE GRIS, J. Geophys. Res. Earth Surf., 121, 223–240, https://doi.org/10.1002/2015JF003601, 2016.

Röthlisberg, H.: Studies in Glacier Physics on the Penny Ice Cap, Baffin Island, 1953: Part III: Seismic Sounding, J. Glaciol., 2, 539–552, https://doi.org/10.3189/002214355793702064, 1955.

Röthlisberger, H.: Water Pressure in Intra- and Subglacial Channels, J. Glaciol., 11, 177–203, https://doi.org/10.3189/S0022143000022188, 1972.

Schoof, C.: The Effect of Cavitation on Glacier Sliding, Proc. Math. Phys. Eng. Sci., 461, 609–627, 2005.

Schoof, C.: Ice sheet grounding line dynamics: Steady states, stability, and hysteresis, J. Geophys. Res. Earth Surf., 112, https://doi.org/10.1029/2006JF000664, 2007.

Togaibekov, A., Le Bris, T., Le Meur, E., Barruol, G., Gimbert, F., Zigone, D., & Lombardi, D.: GNSS data at the Astrolabe Glacier, Zenodo [Data set], https://doi.org/10.5281/zenodo.14003385, 2024

The ObsPy Development Team: ObsPy 1.4.0, Zenodo [Software], https://doi.org/10.5281/zenodo.6645832, 2022

Thelen, W. A., Allstadt, K., Angelis, S. D., Malone, S. D., Moran, S. C., and Vidale, J.: Shallow repeating seismic events under an alpine glacier at Mount Rainier, Washington, USA, J. Glaciol., 59, 345–356, https://doi.org/10.3189/2013JoG12J111, 2013.

Vaughan, D. G.: Investigating tidal flexure on an ice shelf using kinematic GPS, Ann. Glaciol., 20, 372–376, https://doi.org/10.3189/1994AoG20-1-372-376, 1994.

Walker, R. T., Parizek, B. R., Alley, R. B., Anandakrishnan, S., Riverman, K. L., and Christianson, K.: Ice-shelf tidal flexure and subglacial pressure variations, Earth Planet. Sci. Lett., 361, 422–428, https://doi.org/10.1016/j.epsl.2012.11.008, 2013.

Walter, J. I., Svetlizky, I., Fineberg, J., Brodsky, E. E., Tulaczyk, S., Grace Barcheck, C., and Carter, S. P.: Rupture speed dependence on initial stress profiles: Insights from glacier and laboratory stick-slip, Earth Planet. Sci. Lett., 411, 112–120, https://doi.org/10.1016/j.epsl.2014.11.025, 2015.

Winberry, J., Anandakrishnan, S., Wiens, D. A., and Alley, R. B.: Nucleation and seismic tremor associated with the glacial earthquakes of Whillans Ice Stream, Antarctica, Geophys. Res. Lett., 40, 312–315, https://doi.org/10.1002/grl.50130, 2013.

Winberry, J. P., Anandakrishnan, S., and Alley, R. B.: Seismic observations of transient subglacial water-flow beneath MacAyeal Ice Stream, West Antarctica, Geophys. Res. Lett., 36, L11502, https://doi.org/10.1029/2009GL037730, 2009.

https://doi.org/10.5194/egusphere-2026-76
Preprint. Discussion started: 16 February 2026

Winder, T., Bacon, C. A., Smith, J. D., Hudson, T., Greenfield, T., and White, R. S.: QuakeMigrate: a Modular, Open-Source Python Package for Automatic Earthquake Detection and Location, 2020.

Wittlinger, G. and Farra, V.: Observation of low shear wave velocity at the base of the polar ice sheets: evidence for enhanced anisotropy, Geophys. J. Int., 190, 391–405, https://doi.org/10.1111/j.1365-246X.2012.05474.x, 2012.

Yan, P., Holland, D. M., Tsai, V. C., Vaňková, I., and Xie, S.: Tidally Modulated Glacial Slip and Tremor at Helheim Glacier, Greenland, Geophys. Res. Lett., 51, e2023GL105342, https://doi.org/10.1029/2023GL105342, 2024.

Zoet, L. K., Anandakrishnan, S., Alley, R. B., Nyblade, A. A., and Wiens, D. A.: Motion of an Antarctic glacier by repeated tidally modulated earthquakes, Nat. Geosci., 5, 623–626, https://doi.org/10.1038/ngeo1555, 2012.